Biomed Microdevices
DOI 10.1007/s10544-012-9701-4

Chemotactic steering of bacteria propelled microbeads

Dongwook Kim · Albert Liu · Eric Diller · Metin Sitti

Abstract Flagellated bacteria have been embraced by the micro-robotics community as a highly efficient microscale actuation method, capable of converting chemical energy into mechanical actuation for microsystems that require a small payload and high rate of actuation. Along with being highly motile, *Serratia marcescens* (*S. marcescens*), our bacterium species of interest, is a highly agile biomotor capable of being steered via chemotaxis. In this paper, we attached *S. marcescens* bacteria to polystyrene microbeads towards creating biohybrid that can propel themselves towards an attractive chemical source. Using a three-channel microfluidic device, linear chemical gradients are generated to compare the behavior of bacteria-propelled beads in the presence and absence of a chemoattractant, L-aspartate. We tested and compared the behavior of three different bacteria-attached bead sizes (5, 10 and 20 μm diameter) using a visual particle-tracking algorithm, and noted their behavioral differences. The results indicate that in the presence of a chemoattractant, the *S. marcescens*-attached polystyrene beads exhibit a clear indication of directionality and steering control through the coordination of the bacteria present on each bead. This directionality is observed in all bead size cases, suggesting potential for targeted payload delivery using such a biohybrid micro-robotic approach.

Keywords S. marcescens · Micro-robotics · Chemotaxis · Bacterial propulsion

Electronic supplementary material The online version of this article (doi:10.1007/s10544-012-9701-4) contains supplementary material, which is available to authorized users.

Dongwook Kim and Albert Liu are equally contributing authors.

D. Kim · E. Diller
Department of Mechanical Engineering,
Carnegie Mellon University,
Pittsburgh, PA 15213, USA

D. Kim
e-mail: dkim2@andrew.cmu.edu

E. Diller
e-mail: ediller@cmu.edu

A. Liu
Department of Biomedical Engineering,
Carnegie Mellon University,
Pittsburgh, PA 15213, USA
e-mail: albertliu@cmu.edu

M. Sitti (✉)
Department of Mechanical Engineering and Robotics Institute,
Carnegie Mellon University,
Pittsburgh, PA 15213, USA
e-mail: msitti@andrew.cmu.edu

1 Introduction

The recent prominence of miniature mobile robots has been the result in the scaling down of existing robotic agents. Many envision micro-robots able to carry out tasks in small spaces that traditional robots would otherwise be unable to execute successfully. However, the miniaturization of existing systems can exhibit bottlenecks when it comes to creating viable actuation and power sources necessary for effective and efficient mobility at the microscale in mobility, power and control (Sitti 2009).

A number of actuation techniques have been proposed to enable the development of untethered micro-robots. The first of two methodologies utilizes external sources for actuation and power. In one approach, an electrostatically actuated robot was created which utilizes a patterned substrate for remote power delivery and control (Donald et al. 2006), while other groups have delivered such power and control using an externally-generated magnetic field for actuation (Pawashe et al. 2009; Yesin et al. 2006; Diller et al. 2012a, 2012b, 2011; Pawashe et al. 2012; Floyd et al. 2011). However, these

Published online: 09 September 2012

micro-robots can only operate within a limited workspace and require bulky and complex external instrumentation. The second, more recent methodology, utilizes cells or microorganisms such as bacteria and algae for on-board actuation of micro-robots (Darnton et al. 2004; Steager et al. 2007; Kim and Breuer 2007; Weibel et al. 2005; Martel et al. 2009; Leonardo et al. 2010). With simple nutrients such as glucose, biomotors of these biological entities are capable of converting chemical energy to mechanical energy with high efficiency. More importantly, scientists can exploit the integrated sensors and complex behaviors already present within the cell body to control cell and micro-robot movement. While such a bio-hybrid approach has many advantages when compared to off-board actuation methods at tens of micron or smaller scale, there are also new challenges introduced. In particular, the limited actuation duration due to the limited lifetime of cells, the sensitivity of cell motility to environmental and cultivation conditions, the potential pathogenic effects of some cell types for future potential medical applications, and the coordination of the stochastic behavior of large number of cells and micro-robots are all problems which need to be addressed for such biohybrid approaches to become feasible.

Serratia marcescens (*S. marcescens*) is a multi-flagellated bacterium species that is highly agile and efficient swimmer at viscous low Reynolds number environments. Moreover, the sensors within the bacterium can allow for steering via chemotaxis or phototaxis (Steager et al. 2007). The use of *S. marcescens* for micro-scale manipulation and actuation has been well documented in a variety of applications. For example, *S. marcescens* was used to accomplish active mixing by adsorbing swarmer cells onto polydimethylsiloxane (PDMS) surfaces, and also for the propulsion of microscale objects by attaching them to the microobject surface (Darnton et al. 2004). With an ultraviolet light source, *S. marcescens* was also able to accomplish active mixing in microfluidic channels, as well as the propulsion of PDMS microbarges by the same bacteria (Steager et al. 2007; Kim and Breuer 2007) via phototaxis. Behkam and Sitti explored the behavior of bacteria-propelled objects of various geometries in a static fluid, in addition to investigating a chemical switching method to establish on/off control of the bacteria-propelled objects (Behkam and Sitti 2007; Behkam and Sitti 2008). Moreover, to reduce cancelling forces from attached on opposite sides of each micro-object, they proposed chemical and physical patterning techniques to allow for controlled bacteria adhesion in order to achieve higher speeds and more directional motion trajectories (Behkam and Sitti 2008, 2009).

This paper investigates the chemotactic steering behavior and the increased directionality of *S. marcescens* propelled micro-beads when placed in a uniformly linear chemical gradient. Such a linear chemical gradient method is selected because it enables a uniform chemical gradient across the entire microfluidic channel for long durations. In addition, it allows for repeatable and precise gradients to be created, allowing for better analysis than point source based circular chemical gradients, which were used in previous work (Kim et al. 2011). Three different bead sizes are used to compare differences in bacteria-attached bead behavior, both with and without the presence of the chemoattractant, L-aspartate. Here, L-aspartate is selected as the chemoattractant as different from our previous study (Kim et al. 2011) because it provides increased attraction for flagellated bacteria (Park et al. 2003) and it has higher diffusion coefficient, which makes experimental preparation time shorter. Using visual tracking software, the displacement of each bead was recorded and analyzed to determine displacement, speed, and directionality results.

2 Methods and materials

2.1 Bacteria cultivation

The bacteria, *S. marcescens* (ATCC 274, American Type Culture Collection, Manassas, VA), were first grown in nutrient broth (25 g Difco LB Miller Broth and 1 L deionized (DI) water, pH 7.0) for 4 h at 37 °C. A 2 μL aliquot was placed on one end of a nutrient agar plate (25 g Difco LB Miller Broth, 6 g Bacto Agar, 5 g glucose, and 1 L DI water, pH 7.0) and incubated at 30 °C for 14 to 18 h (Kim et al. 2010). After bacteria swarming behavior developed, the inoculation site generally contained a pink pigmentation, exclusive to *S. marcescens*. The swarming colony spanned across the plate with the most motile bacteria faintly pigmented and located along the leading edge of the swarm, as shown in Fig. 1.

2.2 Polystyrene bead preparation

Polystyrene beads were prepared for bacteria attachment through a cleaning process. An aliquot of polystyrene microbeads (Fluka, Sigma-Aldrich, Germany) was first diluted in DI water 5 times from the initial concentration of 10 % by volume. Because these beads are supplied with a surfactant coating, we performed a mild cleaning procedure to remove the surfactant and allow the bacteria to bind to the bead surface (Behkam and Sitti 2008). The bead suspension was centrifuged and re-suspended in 1:1 DI water/Isopropyl alcohol (50 % IPA). The wash procedure was repeated five times to ensure removal of the adsorbed surfactant. After the cleaning sequence, the beads were placed in 1 ml of motility medium (0.1 M potassium phosphate tribasic, 10^{-4}M ethylenediaminetetraacetic acid (EDTA), 0.067 M sodium chloride, 0.01 M glucose, and 0.002 % Tween-20, pH 7.0) (Adler and Templeton 1967). The beads were then concentrated five-fold in preparation for bacteria attachment. This

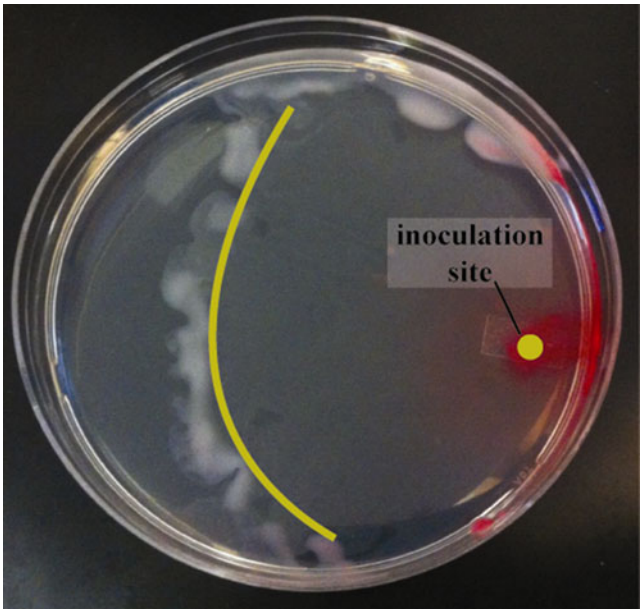

Fig. 1 Top-view photograph of swarming *S. marcescens* on a nutrient agar plate. The most pigmented area on the right marks the inoculation site (denoted by the *yellow* circle), while the leading edge is seen slightly over halfway across the plate. The polystyrene beads are placed for bacteria attachment near the leading edge, marked by the *yellow* line, where the bacteria are the most motile

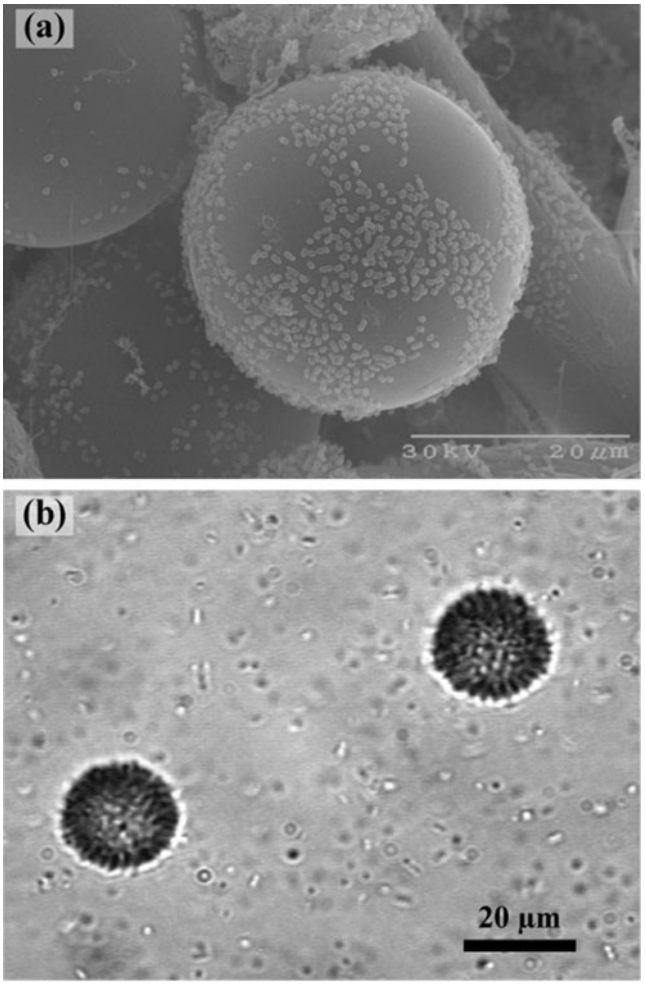

Fig. 2 Images of *S. marcescens*-attached polystyrene microbeads: (**a**) Scanning electron microscope (SEM) image of 30 μm diameter beads with attached bacteria. The individual bacteria are seen as small dots on the smooth surface of the bead. (**b**) Inverted optical microscopic image (using a 40× oil immersion objective lens) of 20 μm diameter beads suspended in motility medium. Attached bacteria can be seen roughly as black spots on the bead surfaces

preparation method was performed for all 5, 10, and 20 μm diameter beads.

A 10 μl aliquot of the final suspension was pipetted onto the leading edge of the swarm agar plate. The sample was incubated at room temperature for 5 min. During this time, bacteria randomly interact with the beads and some adhere to the beads through hydrophobic interactions at an approximate density of 1 bacterium/10 μm^2 (Behkam and Sitti 2009), as shown in Fig. 2. After allowing 5 min for binding to occur, the aliquot was pipetted back into 1 ml of motility medium, and the resulting solution is ready for observation.

2.3 Materials for bacterial chemotaxis

Microfluidic chemical gradient generators of two basic types have been proposed in the literature, flow-based and diffusion-based. Flow-based chemical gradient generators excel in creating steady gradients of arbitrary shape but flow can affect the trajectory of free-swimming cells under study. Consequently, flow-based gradient generators are only appropriate for use in studying surface-attached cells. On the other hand, diffusion-based microdevices can generate a chemical gradient without flow, making them appropriate for use on free-swimming microobjects. One simple approach utilizes source and sink microchannels to maintain a 1D in-plane gradient through hydrogel (agarose) layers (Ahmed et al. 2010). A third test channel located between the source and sink contains the bacteria-propelled microbeads and develops the chemical gradient, as shown in Fig. 3. Any out-of-plane chemical gradients created in the test channel will be small, and are neglected in this work.

To create this microfluidic channel setup, a PDMS (Sylgard 184, Dow Corning, Midland, MI) negative mold of the channels was first fabricated. To do this, the three-channel pattern was laser etched into a 150 μm thick acrylic film. This positive mold was then mounted to the base of an empty petri dish and an 8 mL PDMS solution was poured into the dish and cured at 30 °C for 24 h. The PDMS was then removed to serve as a positive mold.

The procedure to create the experimental platform with the agarose-based channels is illustrated in Fig. 4: (1) The PDMS positive mold was placed on a non-stick polypropylene surface, and a PDMS spacer of thickness 300 μm was placed on top of the mold; (2) An aqueous solution of

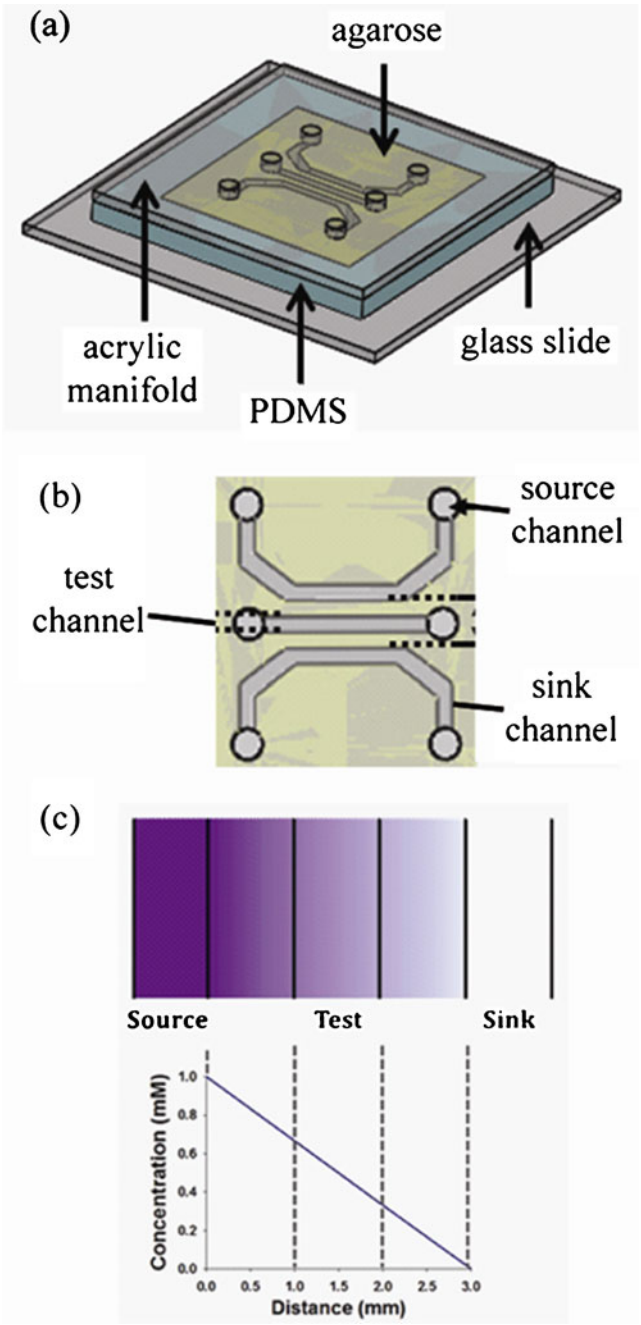

Fig. 3 Schematic of the imaging enclosure: (**a**) In order from bottom to top, 1: glass slide, 2: thin PDMS layer, 3: agarose shaped with three channels, and 4: acrylic manifold with six holes for access to channel inlets and outlets. (**b**) Channel layout of diffusion-based chemical gradient generator, from top to bottom: chemoattractant microchannel (as source), test microchannel (for placement of microbeads), and deionized water microchannel (as sink). (**c**) Illustration of chemoattractant concentration based on distance from the source channel on the chemical gradient generator

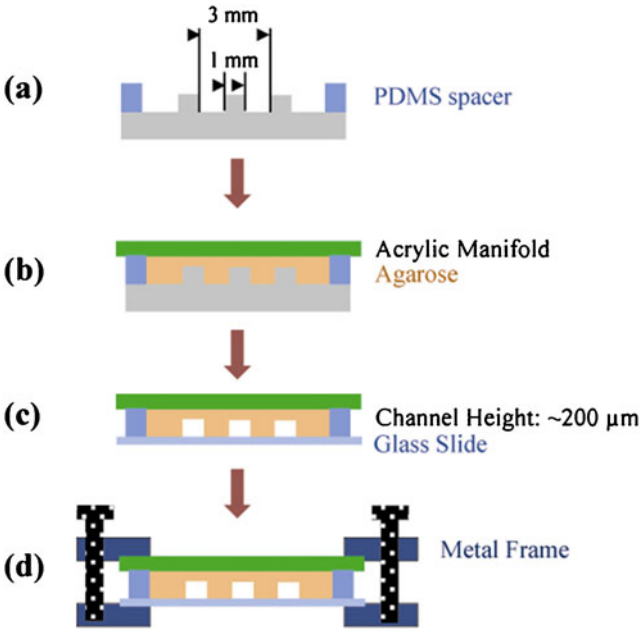

Fig. 4 Step-by-step preparation of three-channel chemical gradient generator, similar to design by Cheng et al.: (**a**) A PDMS spacer is placed on top of a PDMS positive mold to create a reservoir for hot agarose. (**b**) Upon placement of hot agarose, the setup is covered by an acrylic manifold, ensuring that the inlet and outlet holes line up with those on the positive mold. (**c**) After the agarose is given sufficient time to gel (~10 min), the PDMS positive mold is removed. Holes are then created for solution insertion, and the exposed side is covered by a glass slide. (**d**) The final enclosure is then sandwiched together and mounted between two metal frames for secure insertion of solutions

agarose (40 g Eiken Agar and 1 L DI water) was heated on a hot plate and poured in the area enclosed by the spacer. The agarose was promptly covered by a 1 mm thick Plexiglas manifold containing holes at the inlets and outlets of each of the 3 channels. Care was taken to make sure that the inlets and outlets were aligned with those on the PDMS positive mold; (3) After allowing 10 min for the agarose to gel sufficiently, the platform was flipped, and the PDMS positive mold was removed, exposing the channels. To allow insertion of solution into each channel, a 1.8 mm diameter capillary tube (Kimble Glass, KIMAX-51, Vineland, NJ) was used to puncture a hole at the inlets and outlets of each channel through the agarose to the holes on the Plexiglas manifold. (4) Lastly, the exposed channels were sealed by a glass slide, and the platform flipped back upright. In order to ensure proper adherence between layers and to prevent leakage between channels, the platform was lightly squeezed between two aluminum mounting brackets to sandwich the layers together (Cheng et al. 2007).

Upon mounting the platform, 10 µl motility medium was inserted in the test channel and observed briefly to ensure no leakage into other channels. Upon seal confirmation, 10 µl of a 10^{-3} ML-aspartate (chemoattractant) solution was inserted into the source channel, and 10 µl motility medium was inserted into the sink channel. Diffusion of 10^{-4}M fluorescein at such a concentration through agarose has been characterized by Cheng et al., and was shown to effectively diffuse linearly, given a sufficiently low concentration under

10^{-3}M. Therefore, we utilized a 1 mML-aspartate concentration for our application (Cheng et al. 2007). Given the dimensions of the channels, the chemoattractant was given approximately 90 min to diffuse through the test channel and generate a uniformly linear chemical gradient.

Following the linear chemical gradient generation, a small aliquot of bacteria-attached beads was placed in the test channel. Upon placement into the channel, the apparatus was left for 10 min to allow the test channel flow to settle, and for the chemoattractant gradient to restore itself through the test channel. In order to maintain the chemoattractant gradient, 10–20 μl chemoattractant solution or motility medium was placed in their corresponding channels approximately every 20 min (Cheng et al. 2007).

To ensure that free-swimming background bacteria within the bacteria-attached PS bead solution do not engage in collective behavior and consequently affect the movement of the beads themselves, we diluted the bead solution with motility medium to reduce the concentration of background bacteria. In a study on the concentration dependency of dynamic collective behavior, it was shown that for density numbers (volume fraction) under 0.14, no collective behavior is observed (Sokolov et al. 2007). In our experiments, we diluted the various bead solutions accordingly to ensure background bacteria density under 0.14.

2.4 Visual tracking of microbeads

For non-chemotactic experiments, the source and sink channels were both filled with motility medium, while the polystyrene beads were placed in the test channel. For chemotactic experiments, the source and sink channels were filled with chemoattractant and DI water, respectively. The motion of the bacteria-attached PS beads was observed via using an inverted optical microscope (Axiovert 100, Zeiss, Germany) under 20× and 32× objective lenses, as well as a 40× oil immersion objective lens (Zeiss, Germany). Videos were recorded at 23 frames per second for each bead sample using a CCD camera (WV-CD110-A, Panasonic, Japan). These videos were processed in Image J, using a particle tracking plugin (free software and plugin available from NIH, http://rsbweb.nih.gov/ij/), and the trajectory data output from the plugin was analyzed in MATLAB to determine bead mean speeds and directionality information.

2.5 Mean speed calculation

In the test channel, microbeads exhibited different behaviors based on whether they were in contact with the glass bottom surface or floating free in the bulk of the liquid. When near the surface, the beads exhibited a wall effect due to very low Reynolds number regime and were consequently slower in speed; when the beads were further than a few times the bead's diameter away from the surface, the beads tended to be faster, as they were less influenced by the wall effect (Goldman et al. 1967). When the beads were first placed in the test channel, the liquid within the channel exhibited a high flow rate, and the bead trajectories could not be accurately measured. After approximately 10 min, the flow stopped and the chemical gradient was stable throughout the channel. Moreover, by the end of this waiting period, the beads tended to settle near the glass. Therefore, for both non-chemotactic and chemotactic experiments, the beads were observed near the surface only.

When analyzing stochastic random motions of living cells, a metric called the mean square displacement L^2 is used. This metric examines the mean distance travelled by the bead as a function of the observation time duration, averaged over the entire observation period. The mean square displacement allows for the comparison of diffusion and other causes of motion in such randomly driven systems. For our chemotactic bead behavior study, we examined the bead behavior for three different bead diameter sizes: 5 μm, 10 μm, and 20 μm. For both non-chemotactic and chemotactic cases, these beads were coated with bacteria, observed under an optical microscope for a duration lasting 30 s, and subsequently tracked to determine the mean square displacement of each bead as a function of time. The two dimensional (2D) displacement of bacteria propelled beads follows the general equation (Arabagi et al. 2011; Behkam and Sitti 2008; Howse et al. 2007)

$$< \Delta L^2 >= 4D\Delta t + \frac{V_{mean}^2 \tau_R^2}{2}\left[\frac{2\Delta t}{\tau_R} + e^{-\frac{2\Delta t}{\tau_R}} - 1\right], \quad (1)$$

where Δt is the time duration, V is the mean bead velocity, D is the bead diffusion coefficient and τ_R is the randomization time. Here, the first term $4D\Delta t$ of Eq. (1) represents the diffusion of a non-propelled bead in 2D. The second term is the active self-propulsion based translation and rotational stochastic bead motion. Here, the randomization time is $\tau_R = 8\pi\eta R^3/(k_B T)$, where η is the liquid dynamic viscosity, R is the bead radius, and k_B is the Boltzmann constant. The bead will experience rotational diffusion with characteristic rate of τ_R. In this case, τ_R is around 1.4, 11 and 88 min for bead diameters of 5, 10 and 20 μm, respectively. When t is much larger than τ_R, the diffusion term $4D\Delta t$ will dominate the bead's motion, resulting in Brownian motion with a given effective diffusion constant D. However, when t is much smaller than τ_R, the diffusion term can be neglected and Eq. (1) can be approximated as

$$< \Delta L^2 > \approx V_{mean}^2 (\Delta t)^2. \quad (2)$$

In this regime, the mean square displacement should increase with the square of the time duration Δt (Howse et al. 2007).

The specific bead tracking duration of 30 s was chosen to ensure accuracy in tracking while maintaining an observation window well under τ_R (Behkam and Sitti 2009). Thus, by

assuming Δt is much smaller than τ_R and fitting Eq. (2) to data of the mean squared displacement of each bead as a function of Δt, we determined the mean speed V_{mean} of each stochastically propelled bead. Mean square displacement L^2 for a given time duration Δt is calculated from raw position data by stepping through each datapoint and finding the square of the magnitude of the 2D displacement at a time Δt later, and averaging all of these displacements over the entire observed path.

3 Experimental results

To accurately analyze the bead behavior and establish a baseline for chemotactic experiments, we first tracked the motion of bacteria-attached beads in the absence of a chemoattractant for three different bead sizes. These experiments were conducted in a small fluid well with PDMS sides and glass bottom and top. These beads were tracked while near the bottom glass slide surface, resulting in reduced motility due to wall effects between the bacteria-attached bead and the glass surface at the bottom of the experimental apparatus. The trajectories of ten beads of each size for a 30 s duration are illustrated in Fig. 5(a)-(c). Each bead is represented by a different color on the graph, and the starting points of each are denoted by a double concentric circle.

The bead motion is summarized by the mean square displacement, as calculated using the methods from the previous section. The mean square displacements of all beads tracked in the non-chemotactic case are shown in Fig. 6(a)-(c). By fitting a parabola to each trajectory, the mean velocity V_{mean} can be found as in Eq. (2). Also shown in the insets of Fig. 6 are the directionality histograms, taken with a Δt of 2.2 s, showing the tendency of the bead to move in any particular direction. For each frame in the captured video, the bead exhibits a displacement, which can be quantified by a vector. The angles of these each vector are calculated with respect to the chemoattractant, located at the bottom of the frame, and plotted on the histogram. To minimize pixel discretization errors in this directionality calculation, a relatively large Δt of 2.2 s was used.

The mean speeds and standard deviations of each bead throughout different durations are organized by bead size and shown in Table 1. Here, different sizes of beads were investigated because it is important to understand and quantify the scaling effects of bacteria propelled micro-robotic systems where such micro-robots could require larger payloads or any additional on-board components.

In the presence of a chemoattractant, *S. marcescens* bacteria attached to the beads are expected to propel the beads up the chemical gradient, towards the source of the chemoattractant. As described previously, a diffusion-based three-channel agarose chemoattractant gradient generator was fabricated to generate a uniformly linear gradient throughout the width of the test channel (Cheng et al. 2007). By maintaining a flow in the source and sink channels, the chemical continually diffuses through the agar and test channel, maintaining the gradient. Each bead sample was tracked for 30 s, as plotted in Fig. 5 (d)-(f), with respect to their own starting positions within the capture frame, and superimposed upon each other.

The chemotactic nature of the bacteria-attached beads under the influence of a chemical gradient is most clearly illustrated in Fig. 6, which illustrates angle histograms based on 30 s trajectory data from all bead samples, based on bead size. The calculated mean speeds V_{mean} for each bead size for the chemotactic case and their standard deviations are shown in Table 1 along with the non-chemoattractive cases.

Example typical non-chemotactic and chemotactic bead propulsion videos are shown in the supporting documents.

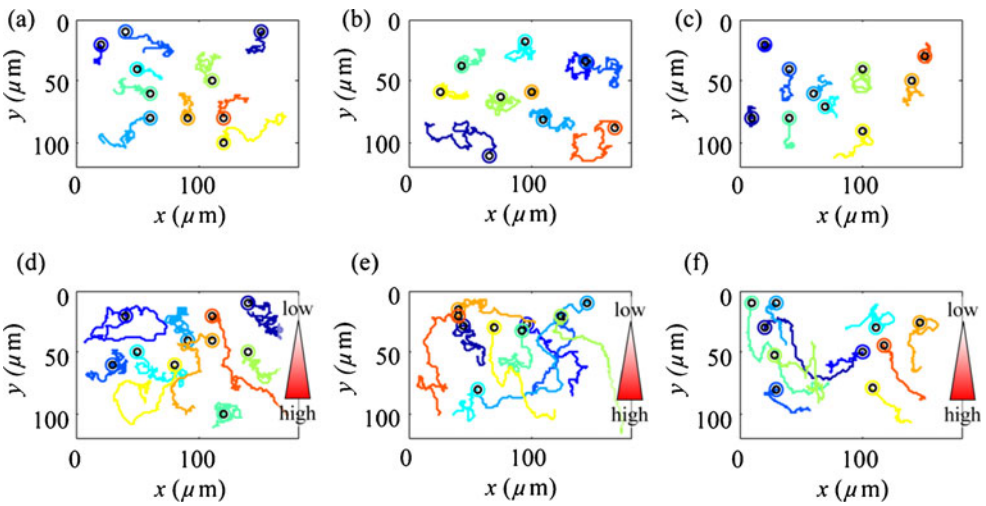

Fig. 5 Trajectory maps of *S. marcescens*-attached microbeads through a duration of 30 s: Non-chemotactic behavior of (**a**) 5 μm, (**b**) 10 μm, and (**c**) 20 μm diameter microbeads; chemotactic behavior of (**d**) 5 μm, (**e**) 10 μm, and (**f**) 20 μm diameter microbeads. For chemotactic behavior, the chemoattractant source is located at the bottom of each map. The starting point of each bead trajectory is marked by a double concentric circle

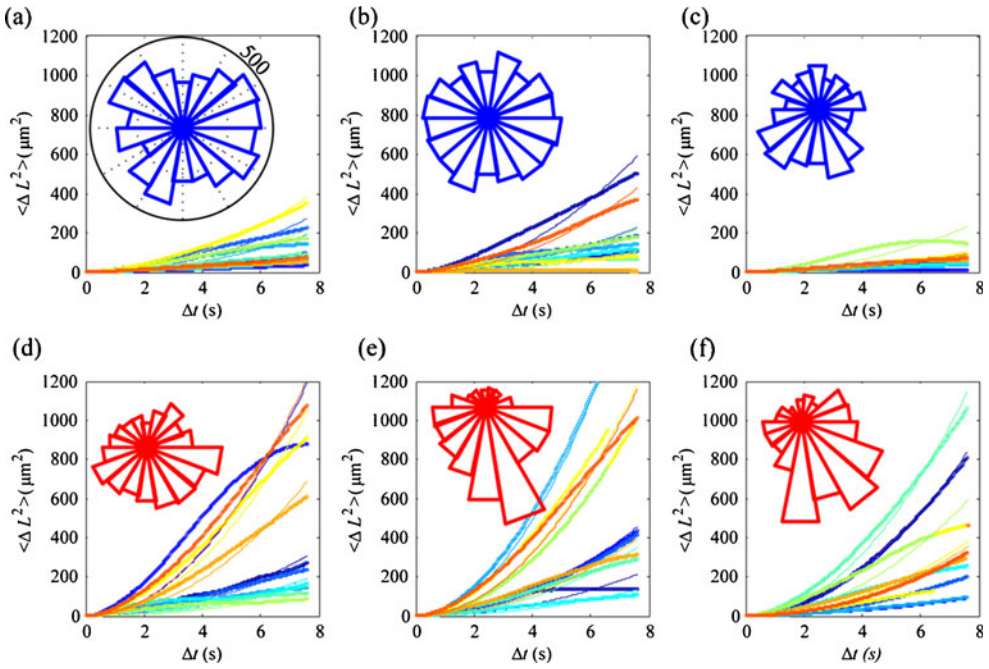

Fig. 6 Mean square displacement of *S. marcescens*-attached microbeads through a duration of 30 s: Non-chemotactic behavior of (**a**) 5 μm, (**b**) 10 μm, and (**c**) 20 μm diameter microbeads; chemotactic behavior of (**d**) 5 μm, (**e**) 10 μm, and (**f**) 20 μm diameter microbeads. Insets show angle histograms of bead directionality, taken with a Δt of 2.2 s. In the absence of chemoattractant, the beads exhibit no preferential direction, and therefore the corresponding angle histograms show a fairly uniform distribution among all angles. However, in the presence of a chemoattractant, the beads have a tendency to move towards the chemoattractant source, located at the bottom of the frame. As seen on the chemotactic angle histograms, there is a peak near the bottom, indicating an increased directionality towards the chemoattractant source

4 Discussions

The large variance in a single bead size's speed, shown in Table 1, is due to the random stochastic nature of the actuation method, and could be largely explained by noting that the number of bacteria attached to each bead can vary widely. As seen in Fig. 2(a), the bacteria do not completely cover the bead surface, and random distribution and number of bacteria could have a large effect on bead speed, as studied previously (Behkam et al. 2008). For each non-chemotactic and chemotactic case, all sample data within one bead size was taken within a single bacterial cultivation. If samples were from different bacterial cultivations, we would expect to see even greater standard deviation for mean speed.

Table 1 Mean speed V_{mean} and standard deviation of 5, 10, and 20 μm diameter bacteria-attached bead propulsion for chemoattractive and non-chemoattractive cases, taken from 10 different bead trajectories each tracked over 30 s

Bead diameter	5 μm	10 μm	20 μm
Non-chemoattractive	1.55±0.56 μm/s	1.81±0.76 μm/s	1.21±0.38 μm/s
Chemoattractive	2.83±1.28 μm/s	3.29±1.31 μm/s	2.59±1.01 μm/s

In Table 1 we see that the mean velocity in the chemotactic case was roughly twice that in the non-chemotactic case, indicating that the presence of the chemical gradient resulted in directed motion along a single direction. In Fig. 5(a)-(c), one can observe that in the absence of a chemoattractant, the beads exhibited no preferential direction of travel. This lack of directionality is characteristic of a random walk like stochastic behavior. However, in Fig. 5(a)-(c), one can observe that in the presence of chemoattractant, the beads did exhibit a preferential downward direction of travel.

For both non-chemotactic and chemotactic cases, the mean speed of each bead size are slightly increasing with bead size, but only to a small extent. While the amount of data is too small here to fully support such a trend, we propose a hypothesis to explain a possible increase in speed with bead size. As the size of the bead increases, the surface area of bead increases as well. However, because our experiments were performed near the glass surface at the bottom of our channels, an increase in contact surface area translates to a greater magnitude of the wall effect. Additionally, while surface area increases with the square of the bead radius and more bacteria are able to attach to the bead surface, propulsive force only increases linearly with radius. As a result, propulsive force

does not scale proportionally with an increase in bead size (surface area).

In the non-chemotactic case, we expect to see a uniform distribution of motion throughout all directions. In the angle histograms of Fig. 6 (a)-(c), we can see that this is primarily the case with all the non-chemotactic bead angle histogram results, due to the fact that there are no pronounced preference in any specific direction. On the other hand, given the presence of a chemical gradient, whose source lies at the lower edge of the channel, we expect the corresponding angle histograms to exhibit a unimodal distribution towards the bottom. As seen in the angle histograms of Fig. 6(d)-(f), each of the three bead sizes show a peak at near the bottom, although the 5 μm bead chemoattractive case shows less downward preference than the 10 and 20 μm beads. A potential explanation for this is that there are fewer bacteria attached to the 5 μm bead than are attached to the 10 and 20 μm beads. It has been shown previously that the number of bacteria can be as low as 1–2 for such a small bead (Behkam and Sitti 2008), which indicates that each individual bacterium is acting independently to push the bead, rather than acting in aggregate. In such a case, the presence of chemoattractant may be overpowered by the random walk characteristics of each individual. Looking at the individual trajectories in Fig. 5(d), we see that some of the beads undergo much more directional motion than others, suggesting that the lack of clear directionality in the aggregate histogram data may be due to some low-performance beads. Such effects must be further studied in future work.

As a final observation, the orientation of individual *S. marcescens* bodies on the bead surface can greatly affect the overall bead motion. As observed in a small percentage of beads, the beads not only exhibited a two-dimensional displacement, but also engaged in a rolling movement not captured in the data presented here, but seen in the experimental videos. If the cell body of the bacterium attaches by its side to the bead, then its "run" mode would contribute more to the rolling motion of the bead rather than its translational motion, which would reduce its translational speed.

5 Conclusions

This paper demonstrated the behavior of *S. marcescens*-attached 5 μm, 10 μm, and 20 μm diameter polystyrene beads in the absence and presence of a chemoattractant, L-aspartate. When no chemoattractant is present, the bacteria-attached beads engage in a stochastic non-directional motion, in accordance with the behavior documented by previous studies. However, when the beads are placed in the presence of a linear chemoattractant gradient, the bead behaviors change. By using a diffusion-based linear microfluidic chemical gradient generator and observing the bead motion, the following conclusions could be made. In the presence of a chemoattractant, the bead motions become significantly straighter, resulting in faster mean bead velocities, which suggests that the run-to-tumble ratio of each individual bacteria is increasing. Through angle histograms of their motion, the bacteria-attached beads have a tendency to move towards the direction of the chemoattractant source, indicating that chemical gradients can act as direction control for bacteria-attached beads. Additionally, in both non-chemotactic and chemotactic cases, as bead size increases, the mean bead speed increases slightly. This was attributed to an increasing proportion of propulsive force over surface area as the bead diameter increases. While other recent results have demonstrated progress in control of individual or swarms of bacteria, this study has shown the first example of directed payload motion driven solely by attached bacteria.

This study has demonstrated the potential for utilizing bacteria-attached micro-beads controlled by bacterial chemotaxis as a passive steering control method for various future biohybrid micro-robotics applications in medicine such as local disease diagnosis and targeted drug delivery and in environmental monitoring. Moreover, through the testing of various microbead sizes, it can be concluded that there exists an optimal micro-robot body size that allows for a balance between propulsive force and wall effects. Improving bead patterning (Behkam and Sitti 2008) and bacteria attachment techniques could further improve the motility and steering capability of the bacteria-propelled microbeads as future works. Finally, because the wall effects reduce the bead speeds close to the glass slide, we will investigate buoyant microbeads that could move without any wall effects far from surfaces.

Acknowledgements The authors of this paper would like to thank the members of the NanoRobotics Laboratory at Carnegie Mellon University for their help and discussions. We would also like to thank Joseph Suhan of Carnegie Mellon University for help in SEM imaging. This work was supported by the NSF CPS-Medium project (CNS-1135850).

References

J. Adler, B. Templeton, J. Gen. Microbiol. **46**, 175 (1967)
T. Ahmed, T.S. Shimizu, R. Stocker, Nano. Lett. **10**, 3379 (2010)
V. Arabagi, B. Behkam, M. Sitti, J. Appl. Phys. **109**, 114702 (2011)
B. Behkam, M. Sitti, Appl. Phys. Lett. **93**, 223901 (2008)
B. Behkam, M. Sitti, Appl. Phys. Lett. **90**, 023902 (2007)
B. Behkam and M. Sitti, Proc. IEEE Int. Conf. Robot., 1022 (2009)
B. Behkam and M. Sitti, Proc. IEEE-RAS-EMBS International Conference on Biomedical Robotics and Biomechatronics, 753 (2008)
S.-Y. Cheng, S. Heilman, M. Wasserman, S. Archer, M.L. Shulerac, M. Wu, Lab on a Chip **7**(763) (2007)
N. Darnton, L. Turner, K. Breuer, H.C. Berg, Biophys. J. **86**, 1863 (2004)
E. Diller, S. Floyd, C. Pawashe, M. Sitti, IEEE Trans. on Robotics **28**, 172 (2012a)

E. Diller, S. Miyashita, M. Sitti, RSC Advances **2**, 3850 (2012b)
E. Diller, C. Pawashe, S. Floyd, M. Sitti, Int. J. Robot. Res. **30**, 1667 (2011)
B. Donald, C. Levey, C. McGray, I. Paprotny, D. Russ, J. Microelectromech. S. **15** (2006)
S. Floyd, E. Diller, C. Pawashe, M. Sitti, Int. J. Robot. Res. **30**, 1553 (2011)
A.J. Goldman, R.G. Cox, H. Brenner, Chem. Eng. Sci. **22**(4), 653 (1967)
J.R. Howse, R.A.L. Jones, A.J. Ryan, T. Gough, R. Vafabakhsh, R. Golestanian, Phys. Rev. Lett. **99**, 0481021 (2007)
D. Kim, A. Liu, and M. Sitti, Proc. IEEE/RSJ Int. Conf. Robots and Intelligent Systems, 1674 (2011)
D.H. Kim, E.B. Steager, U.K. Cheang, D. Byun, M.J. Kim, J. Micromech. Microeng. **20**, 065006 (2010)
M. Kim, K. Breuer, J. Fluid Eng. – T. ASME **129**, 319 (2007)
R.D. Leonardo, L. Angelani, D. Dell'Arciprete, G. Ruocco, V. Iebba, S. Schippa, M.P. Conte, F. Mecarini, F.D. Angelis, E.D. Fabrizio, P. Natl. Acad. Sci. USA **107**, 9541 (2010)
S. Martel, M. Mohammadi, O. Felfoul, Z. Lu, P. Pouponneau, Int. J. Robot. Res. **28**, 571 (2009)
S. Park, P. Wolanin, E. Yuzbashyan, H.N. Darnton, J. Stock, P. Silberzan, R. Austin, P. Natl. Acad. Sci. USA **100**, 13910 (2003)
C. Pawashe, S. Floyd, E. Diller, M. Sitti, IEEE Trans. on Robotics **28**, 467 (2012)
C. Pawashe, S. Floyd, M. Sitti, Int. J. Robot. Res. **28**, 1077 (2009)
M. Sitti, Nature **458**, 1121 (2009)
A. Sokolov, I. Aranson, J. Kessler, R. Goldstein, Phys. Rev. Lett. **98**, 1581021 (2007)
E. Steager, C. Kim, J. Patel, S. Bith, C. Naik, L. Reber, M.J. Kim, Appl. Phys. Lett. **90**, 263901 (2007)
D.B. Weibel, P. Garstecki, D. Ryan, W.R. DiLuzio, M. Mayer, J.E. Seto, G.M. Whitesides, P. Natl. Acad. Sci. USA **102**, 11963 (2005)
K. Yesin, K. Vollmers, B. Nelson, Int. J. Robot. Res. **25**, 527 (2006)